materials

MDPI

Article

Monoclinic 122-Type $BaIr_2Ge_2$ with a Channel Framework: A Structural Connection between Clathrate and Layered Compounds

Xin Gui [1], Tay-Rong Chang [2], Tai Kong [3], Max T. Pan [1], Robert J. Cava [3] and Weiwei Xie [1,*]

1 Department of Chemistry, Louisiana State University, Baton Rouge, LA 70803, USA; xgui2@lsu.edu (X.G.); maxpan172910@gmail.com (M.T.P.)
2 Department of Physics, National Cheng Kung University, Tainan 70101, Taiwan; u32trc00@phys.ncku.edu.tw
3 Department of Chemistry, Princeton University, Princeton, NJ 08540, USA; taik@princeton.edu (T.K.); rcava@princeton.edu (R.J.C.)
* Correspondence: weiweix@lsu.edu; Tel.: +1-225-578-1074

Received: 26 June 2017; Accepted: 10 July 2017; Published: 18 July 2017

Abstract: A new 122-type phase, monoclinic $BaIr_2Ge_2$ is successfully synthesized by arc melting; X-ray diffraction and scanning electron microscopy are used to purify the phase and determine its crystal structure. $BaIr_2Ge_2$ adopts a clathrate-like channel framework structure of the monoclinic $BaRh_2Si_2$-type, with space group $P2_1/c$. Structural comparisons of clathrate, $ThCr_2Si_2$, $CaBe_2Ge_2$, and $BaRh_2Si_2$ structure types indicate that $BaIr_2Ge_2$ can be considered as an intermediate between clathrate and layered compounds. Magnetic measurements show it to be diamagnetic and non-superconducting down to 1.8 K. Different from many layered or clathrate compounds, monoclinic $BaIr_2Ge_2$ displays a metallic resistivity. Electronic structure calculations performed for $BaIr_2Ge_2$ support its observed structural stability and physical properties.

Keywords: new 122-phase; $BaIr_2Ge_2$; metal-insulator transition (MIT)

1. Introduction

Quasi-two-dimensional (2D) layered intermetallic compounds attract broad interest in condensed matter physics and solid state chemistry for their various physical and structural properties. Some of the most well-known examples are Fe-based superconducting families, such as $FeSe_{1-x}$ [1,2], $LaFeAsO_{1-x}F_x$ [3], and $Ba_{1-x}K_xFe_2As_2$ [4]. In addition to the high temperature superconductors, layered compounds host other strong quantum thermal and spin fluctuations, for example, charge-density-waves (CDWs) [5] and spin-density-waves (SDWs) [6]. Structurally, many two-dimensional layered intermetallics, especially of the 122-type, can be traced back to the parent structure, body-centered tetragonal $BaAl_4$ (space group $I4/mmm$) [7,8]. In $BaAl_4$, the Al atoms, on two independent crystallographic (4*d* and 4*e*) sites, form $Al@Al_4$ tetrahedral layers separated by Ba atoms. Derived from $BaAl_4$, two major ternary intermetallic families are the $ThCr_2Si_2$ and $CaBe_2Ge_2$-types, with 4*d* and 4*e* sites occupied by transition metals (T) and metalloids (M) [9,10]. Identical by symmetry through the body centering, the $ThCr_2Si_2$ structure contains two equivalent T_2M_2 layers per cell. Not only are high T_c Fe-based superconductors known in this structure, but strongly correlated electron behavior and magnetic ordering transitions tuned by chemical and physical pressure are also observed [11]. In contrast to $ThCr_2Si_2$, the primitive tetragonal $CaBe_2Ge_2$ structure consists of alternating T_2M_2 and M_2T_2 layers. Currently, no high T_c superconductors have been reported in the $CaBe_2Ge_2$ structure; but many exotic properties are found for materials in this structure, such as multiple bands leading to the coexistence of charge density waves and superconductivity in $SrPt_2As_2$ [12]. By removing the inversion center from the $BaAl_4$ structure, non-centrosymmetric

$CeCoGe_3$ and $CePt_3Si$ form, for example [13,14], offering hosts to study superconductivity in non-centrosymmetric structures. Finally, clathrates, which form in different, related structure types, are based on frameworks made primarily of Si, Ge, or Sn (with some M included) with the large atoms are found within the framework cages and are generally known to be semiconducting thermoelectrics, although a small number are known to be superconducting [15–17].

The chemical stabilities of many 122-type AT_2M_2 compounds can be interpreted using Zintl-Klemm concepts [18]. In these compounds, the polyanion T_2M_2 layers and intermediary cation layers alternate along the stacking (c) axis. From the chemical perspective, the differences in the electronegativity of the layers determine whether insulating, semiconducting, semimetallic, or metallic behavior is observed [19]. Here, we report our recent discovery of the 122-phase $BaIr_2Ge_2$. The clathrate-like channel framework of $BaIr_2Ge_2$ can be regarded as an intermediate structure between clathrate and the normally layered compounds with 122 stoichiometry. The new structural motif for a heavy metal 122 germanide offers a new platform to study structure-property relationships in such compounds. The crystal structure, basic electronic and magnetic properties, and calculated electronic structure are presented in the following.

2. Experimental

2.1. Synthesis of Monoclinic $BaIr_2Ge_2$

The synthesis of $BaIr_2Ge_2$ was performed by arc melting methods, similar to that used for the synthesis of $BaIrGe_3$ [20]. Starting materials were barium (>99%, rod, Alfa Aesar, Ward Hill, MA, USA), iridium (99.9%, powder, ~325 mesh, Alfa Aesar) and germanium (99.9999%, pieces, Alfa Aesar). The Ir and Ge were weighed in a 1:1 atomic ratio and were arc-melted together under a high purity, Zr-gettered, argon atmosphere. The monoclinic $BaIr_2Ge_2$ phase was obtained by arc-melting the shiny IrGe droplet and Ba pieces (at 50% excess). $BaIr_2Ge_2$ was stored in the glove box due to its sensitivity to both air and moisture. To investigate the phase stability at different temperatures, we put the as-cast samples into an alumina crucible, which were subsequently sealed in an evacuated (10^{-5} torr) quartz tube and were annealed at 800 °C or 1000 °C for four days. After annealing, the $BaIr_2Ge_2$ compound decomposed to IrGe and unidentified phases.

2.2. Phase Identification

Powder X-ray diffraction data was collected using a Rigaku MiniFlex 600 powder X-ray diffractometer (Rigaku, Tokyo, Japan) equipped with Cu K_α radiation (λ = 1.5406 Å, Ge monochromator). A Bragg angle 2θ ranging from 5° to 60° with a 0.01° step with a fast scanning mode was employed due to the air-sensitivity of $BaIr_2Ge_2$. The patterns were analyzed using the LeBail method with Jana2006 [21]. (Lower panel in Figure 1) The calculated pattern in Figure 1 (upper panel) was generated using the crystal structure determined from the single crystal X-ray diffraction results.

2.3. Single Crystal Structure Determination

More than five small single crystals (~0.01 × 0.01 × 0.05 mm^3) from the arc-melted samples of $BaIr_2Ge_2$ were tested to probe the homogeneity of the new phase. A Bruker Apex II diffractometer (Bruker, Billerica, MA, USA) with Mo radiation ($\lambda_{K\alpha}$ = 0.71073 Å) was utilized to analyze the sample. The single crystals protected with glycerol were mounted on a Kapton loop (MiTeGen, New York, NY, USA) and scanned with a 2θ range of 5–65° at room temperature. The exposure time was set as 10 s per frame, and the width of scans was 0.5°. To solve the crystal structure, we used direct methods and full-matrix least-squares on F^2 within the SHELXTL package [22]. Bruker SMART software was applied to make data acquisition, intensity extraction, and corrections for Lorentz and polarization effects [23].

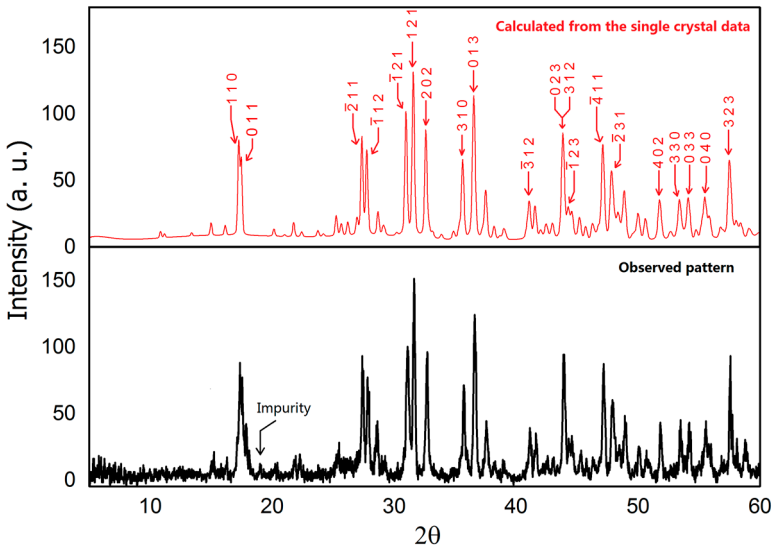

Figure 1. Powder X-ray diffraction pattern of $BaIr_2Ge_2$ (Cu Kα radiation, 300 K). Lower—observed pattern; Upper—calculated pattern with marked Miller indices (hkl) based on the single crystal structure.

2.4. Magnetic Property Measurements

A quantum design physical property measurement system (PPMS) Dynacool (Quantum Design, San Diego, CA, USA) was used to measure the basic magnetic and electronic properties of $BaIr_2Ge_2$. A range from 0 T to 9 T magnetic field at 1.8 K was applied to obtain the field-dependent magnetization. Temperature-dependent magnetization measurements were performed under a magnetic field of 5 T. The 4-probe, zero-field, resistance measurements were carried out in the temperature range from 1.8 K to 300 K.

2.5. Electronic Structure Calculations

Crystal orbital hamilton population (COHP) calculations using the tight-binding linear-muffin-tin-orbital (TB-LMTO) method were performed to analyze the atomic interactions in $BaIr_2Ge_2$ and its chemical stability. The *k*-point mesh in the Brillouin zone was set up as $7 \times 8 \times 7$ to perform the calculations. The electronic structures including the density of states (DOS) and the band structure of $BaIr_2Ge_2$ were calculated using the Vienna Ab initio Simulation Package (VASP) based on density functional theory (DFT) [24] with the use of the generalized gradient approximation (GGA) [25]. Spin-orbit coupling (SOC) was included for all the atoms. The cutoff energy was set at 500 eV. A $7 \times 8 \times 7$ Monkhorst-Pack *k*-point mesh with the linear tetrahedron method was used to perform the calculations. The convergence criterion was set to less than 0.1 meV per atom.

3. Results and Discussion

According to previous research, most 122-type compounds involving alkali-earth metals, group 14 elements, and cobalt group elements (Co/Rh/Ir) adopt the body-centered tetragonal $ThCr_2Si_2$-type [18,26–33]. However, only two reported compounds, $BaRh_2Si_2$ and $BaIr_2Si_2$, crystallize in $BaRh_2Si_2$-type structure [34]. Different from $CaBe_2Ge_2$ and $ThCr_2Si_2$, which are of the tetragonal layered unit cell, $BaRh_2Si_2$ structure belongs to the monoclinic system. Our synthetic exploration of $BaIr_2Ge_2$ has $BaRh_2Si_2$ structure type according to the single crystal X-ray diffraction. Their crystal structures will be discussed in a subsequent section.

3.1. Phase Identification and Structure Determination of $BaIr_2Ge_2$

The existence of the new $BaIr_2Ge_2$ phase was first seen through the analysis of the powder X-ray diffraction data. Single crystal X-ray diffraction was then used to determine the chemical structure and compositions of $BaIr_2Ge_2$. The crystal structure determined is similar to that of $BaRh_2Si_2$. The powder XRD pattern was successfully indexed and refined using the crystal structure obtained from single crystal XRD. The refined lattice parameters of $BaIr_2Ge_2$ are slightly larger than the ones observed in $BaIr_2Si_2$, which is reasonable due to the atomic radius difference between Si and Ge. The results of the diffraction investigation are summarized in Tables 1 and 2 which include the atomic positions, site occupancies, and isotropic thermal displacements. Results for refinements using anisotropic thermal displacements are summarized in Table S2 of the Supporting Information. The $BaIr_2Ge_2$ structure crystallizes in the primitive monoclinic space group $P2_1/c$ (No. 14) with 20 atoms per unit cell distributed among five crystallographic sites in each unit cell. Mixed site occupancy models have been tested to show whether the atomic distribution in $BaIr_2Ge_2$ is ordered and stoichiometric. The crystal structure, shown in Figure 2, is based on an Ir-Ge channel filled with Ba atoms. The view along the a-axis, illustrated in Figure 2a, emphasizes the Ba-filled Ir-Ge framework. Each of the Ir atoms is surrounded by four Ge atoms, forming irregular tetrahedra; similarly, Ge atoms are surrounded by four Ir atoms. The Ir-Ge distances range from 2.40 Å to 2.50 Å. The $Ir@Ge_4$ and $Ge@Ir_4$ clusters share edges and form the channel along the *a*-axis. The diameter of the columnar channel is approximately 6.45 Å, which is sufficient for hosting some small chemical molecules (with the Ba removed), such as carbon dioxide and methane.

Table 1. Single crystal crystallographic data for $BaIr_2Ge_2$ at 299 (2) K.

Refined Formula	**$BaIr_2Ge_2$**
Formula weight (F.W.) (g/mol)	666.92
Space group; Z	$P2_1/c$ (No. 14); 4
a (Å)	8.204 (5)
b (Å)	6.625 (4)
c (Å)	7.959 (5)
β (°)	94.27 (1)
V (Å^3)	431.4 (4)
Extinction Coefficient	0.00061 (9)
θ range (deg)	2.489–32.085
hkl ranges	$-12 \leq h \leq 12$ $-9 \leq k \leq 9$ $-11 \leq l \leq 10$
No. reflections; R_{int}	9731; 0.0925
No. independent reflections	1483
No. parameters	47
R_1: ωR_2 (all *I*)	0.0503; 0.0872
Goodness of fit	0.954
Diffraction peak and hole (e$^-$/Å^3)	3.812; −3.705

Table 2. Atomic coordinates and equivalent isotropic displacement parameters for $BaIr_2Ge_2$ in space group $P2_1/c$. U_{eq} is defined as one-third of the trace of the orthogonalized U_{ij} tensor (Å^2).

Atom	**Wyckoff.**	**Occ.**	***x***	***y***	***z***	***U_{eq}***
Ba1	4*e*	1	0.2318 (1)	0.8818 (2)	0.4993 (2)	0.0116 (3)
Ir2	4*e*	1	0.6260 (1)	0.8959 (1)	0.1069 (1)	0.0074 (2)
Ir3	4*e*	1	0.8532 (1)	0.6648 (1)	0.3334 (1)	0.0077 (2)
Ge4	4*e*	1	0.5560 (2)	0.8515 (3)	0.8069 (3)	0.0088 (4)
Ge5	4*e*	1	0.9282 (2)	0.9171 (3)	0.1356 (3)	0.0091 (4)

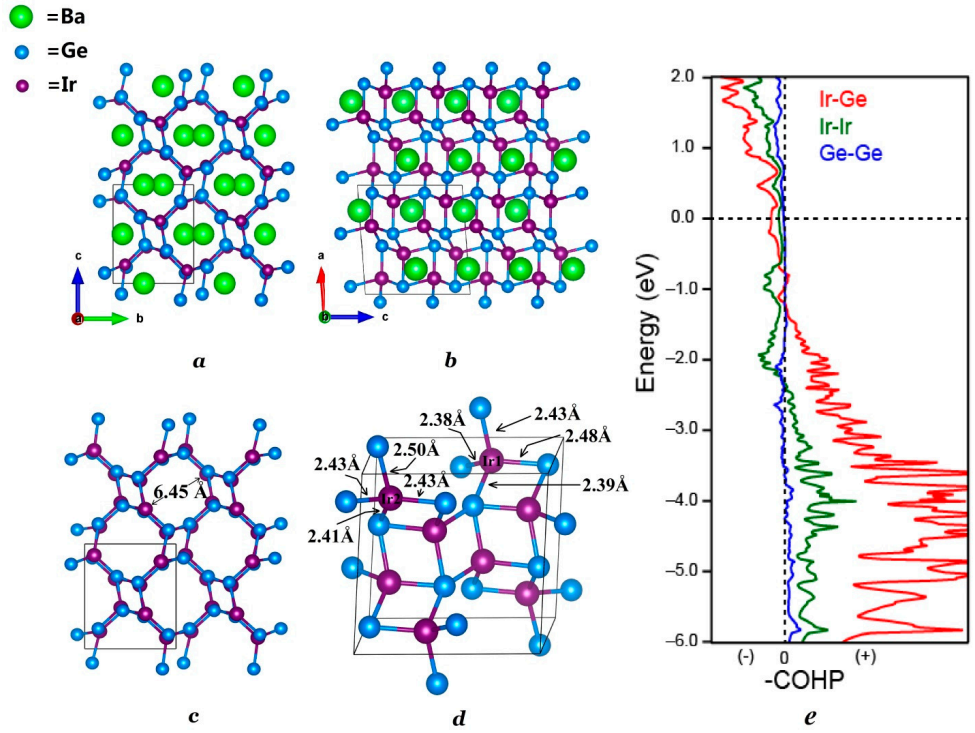

Figure 2. Crystal structure of monoclinic $BaIr_2Ge_2$ refined by single crystal X-ray diffraction. (**a**) View down the a-axis; (**b**) View down the b-axis; (**c**) The IrGe framework. The channels running along the a-axis have a channel of diameter ~6.45 Å; (**d**) close-up of the framework structure showing the Ir-Ge bond lengths; (**e**) Crystal orbital hamilton populations (-COHP) calculation emphasis on the Ir-Ge, Ir-Ir, and Ge-Ge interactions.

3.2. Structural Comparison of the Different 122 Phases

The results of the analysis of the bonding interactions using the crystal orbital hamilton population (COHP) method are shown in Figure 2e. The atomic interactions between Ir and Ge in the Ir-Ge polyanion framework dominate the atomic interactions in $BaIr_2Ge_2$. The Fermi level is located in the non-bonding parts in the COHP, which indicates that the structure of $BaIr_2Ge_2$ is electronically stable.

The combination of alkaline-earth elements, a group of 14 metalloids, and Co group metals (Co/Rh/Ir) in a 122 atomic ratio yields three 122-type phases—the $BaRh_2Si_2$-type (Pearson Symbol, *mP*20), the $ThCr_2Si_2$-type (Pearson Symbol, *tI*10), and the $CaBe_2Ge_2$-type (Pearson Symbol, *tP*10). To estimate the structural preferences, the total energies of $BaIr_2Ge_2$ in different 122-type structures were calculated using WIEN2k codes. According to calculations for the total energies of these structures, the $BaRh_2Si_2$-type gives the lowest energy for $BaIr_2Ge_2$, which agrees with our experimental observations.

3.3. Structural Connections between Clathrate and Layered Compounds

The other interesting ternary compounds in the Ba-Ir-Ge system are the body-centered tetragonal superconductor, $Ba_3Ir_4Ge_{16}$ [35] and non-centrosymmetric tetragonal $BaIrGe_3$ [36]. As shown in Figure 3, Ir-centered square pyramids, symmetrical pentahedra, and irregular, non-symmetrical tetrahedra are formed in $BaIrGe_3$, $Ba_3Ir_4Ge_{16}$, and $BaIr_2Ge_2$, respectively. The crystal structure of the superconductor $Ba_3Ir_4Ge_{16}$ reveals that it contains the unique edge-shared crown-shaped $Ba@Ge_{16}$ polyhedra [35]. The systems with heavy cations "rattling" inside the oversized lattice cavities are called clathrate type structures. Moreover, the open channels around the chains filled with electropositive metals can be considered as clathrate-like structure forms [16]. Accordingly, $BaIr_2Ge_2$ can also be regarded as the clathrate-like compound with Ba rattling inside the open chains, which consist of edge-sharing $Ir@Ge_4$ irregular tetrahedra in Figure 3. One can easily see that $BaIrGe_3$ is a layered

compound with Ir centered in the vertex-sharing Ge square pyramids along the *ab*-plane. Therefore, the clathrate-like $BaIr_2Ge_2$ structure is likely an intermediate structure between regular clathrate and layered structures.

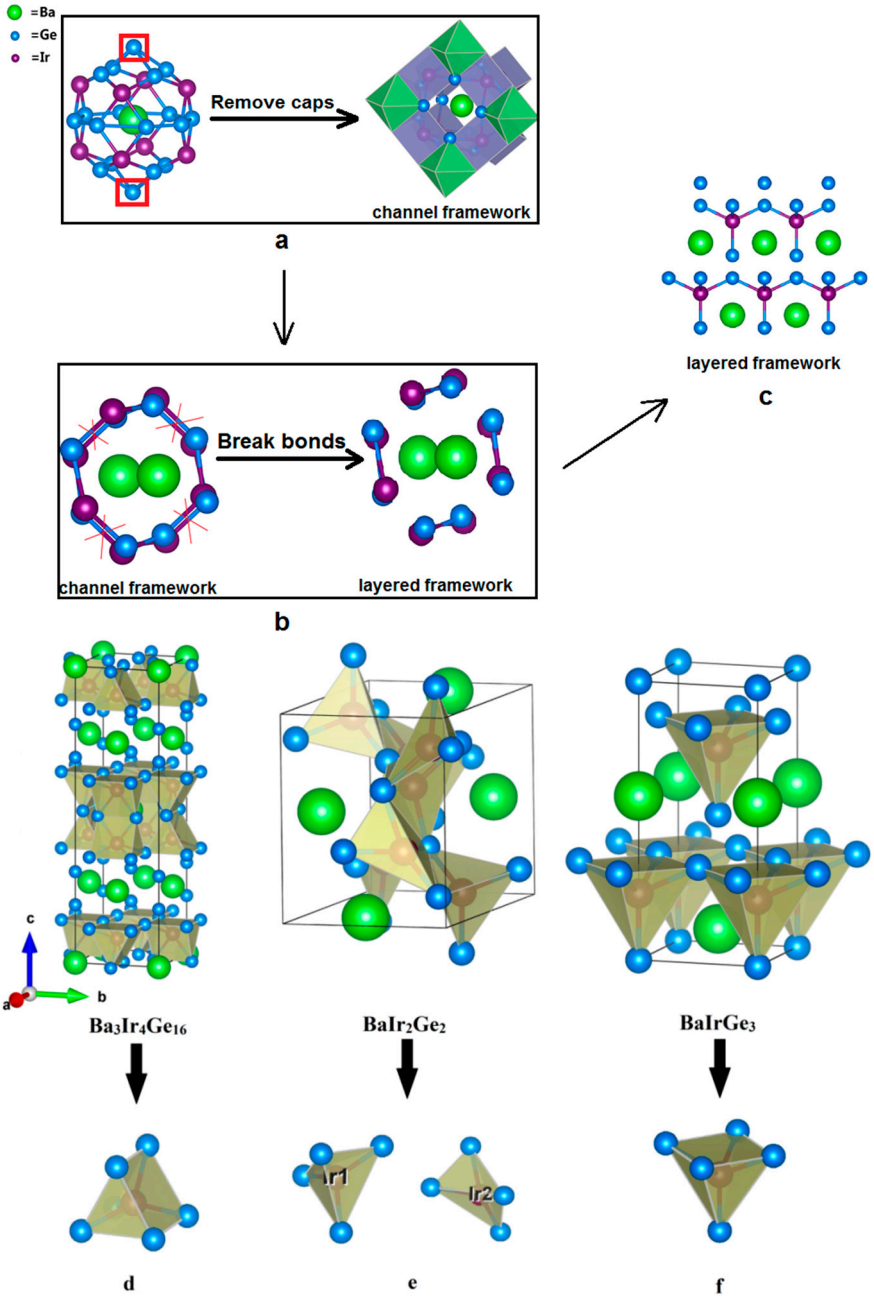

Figure 3. Structural comparison of 122-type phases. (**a**) Clathrate structure of $Ba_3Ir_4Ge_{16}$; (**b**) Channel framework of $BaIr_2Ge_2$; (**c**) Layered structure of $BaIrGe_3$; (**d**) The symmetrical pentahedron in $Ba_3Ir_4Ge_{16}$; (**e**) The irregular, non-symmetrical tetrahedron in $BaIr_2Ge_2$; (**f**) The square pyramid in $BaIrGe_3$.

3.4. Magnetic Properties of Monoclinic $BaIr_2Ge_2$

To further study the physical properties of $BaIr_2Ge_2$, magnetic measurements were carried out. First, no superconductivity was observed above 1.8 K (in low applied field (20 Oe) measurements). Moreover, the relatively small temperature-independent molar magnetic susceptibility, presented

in Figure 4 (Left, Main Panel), is dominated by core diamagnetism; the magnetic susceptibility of the material is around -6×10^{-2} emu/g. The magnetic isotherm measurements in Figure 4 (Left, Inserted) showing diamagnetic behavior at 1.8 K are in agreement with the temperature-dependent magnetization. This indicates that the paramagnetic contribution of conduction electrons to the observed susceptibility is small, which is indirect evidence to support the Zintl-like characteristics of $BaIr_2Ge_2$. The resistance measurements in Figure 4 (Right) show a metallic behavior with a residual resistance ratio of ~ 5.

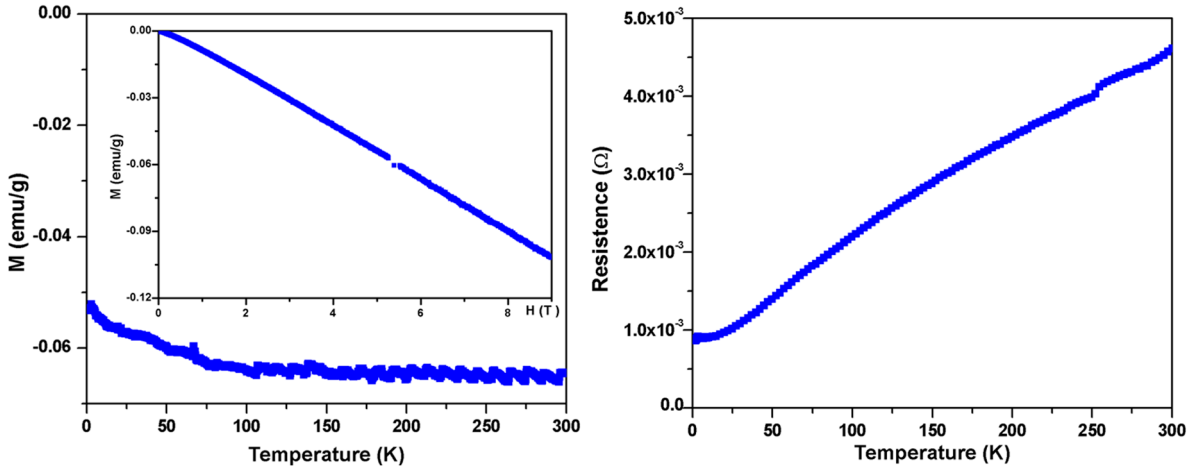

Figure 4. Basic electronic and magnetic characterization of $BaIr_2Ge_2$. (**Left:** Main Panel) Temperature-dependent magnetic susceptibility (M/μ_0H at μ_0H = 5 T) and (**Left:** Inserted) field-dependent magnetization measurements showing the near linearity of M (magnetization) vs. H (magnetic field) for fields beyond 5 T at 1.8 K, justifying the use of the a high applied field in the measurements; (**Right**) Zero-field resistance data from 1.8 K to 300 K.

3.5. Electronic Structure Calculations

Electronic calculations were carried out to evaluate and analyze the electronic density of states (DOS) and band structure, which can help provide a better understanding of the structural stability and physical properties of $BaIr_2Ge_2$. The partial DOS curves (Figure 5a) emphasize the contributions from the valence orbitals of each atom and show that the Fermi level (E_F) lies in a broad pseudo gap in the DOS. This is indicative of the chemical stability of the compound, and also, due to the low density of states, is consistent with the diamagnetism and metallic resistivity observed (see below); no saddle point is seen in the band structure in the vicinity of the Fermi level, making the lack of observed superconductivity above 1.8 K consistent (again, see below) with some ideas for what gives rise to superconductivity in many compounds [37]. Based on the comparison of the electronic structure results with and without the inclusion of spin-orbit coupling, the major impact of the SOC near the E_F is a band splitting into states derived primarily from the 6*s*/5*d* orbitals of the Ir atoms, see Figure 5d. We speculate that doping with electronegative elements like P or A may induce a metal-insulator transition (MIT) in $BaIr_2Ge_2$.

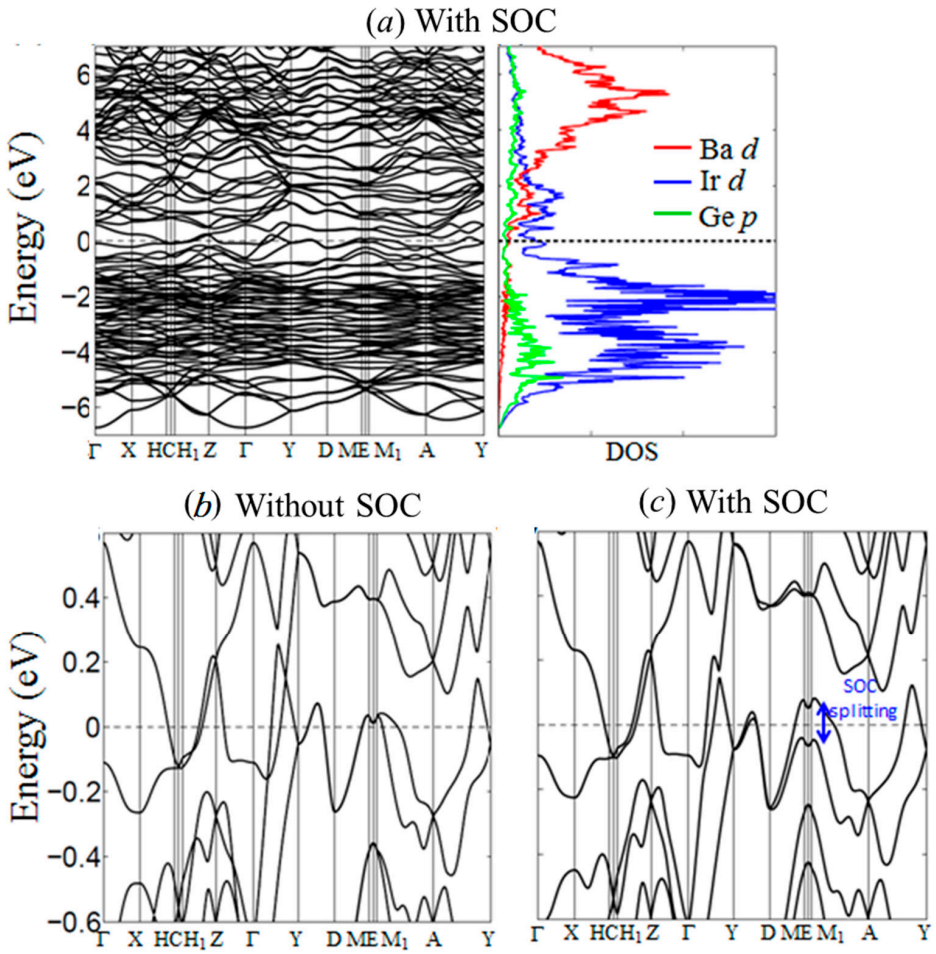

Figure 5. Calculated electronic band structure and density of states (DOS) of $BaIr_2Ge_2$ using generalized gradient approximation (GGA). (**a**) Band structure and DOS with spin-orbit coupling emphasis on the energy range from −7 to +7 eV; (**b**) Band structure calculated by GGA without spin-orbit coupling; (**c**) Band structure calculated by GGA with spin-orbit coupling.

4. Conclusions

The new $BaIr_2Ge_2$ compound, with monoclinic structure $P2_1/c$ (S.G.14), was successfully synthesized using arc-melting. The crystal structure of $BaIr_2Ge_2$ shows a clathrate-like channel framework of Ir-Ge, which can be regarded as an intermediate structure between clathrate and layered compounds. Electronic structure calculations and chemical bonding interactions of $BaIr_2Ge_2$ were investigated to help understand the chemical stability of the compound and its properties. Magnetic measurements indicate diamagnetic susceptibility of $BaIr_2Ge_2$ without the observation of superconductivity down to 1.8 K. The resistivity measurements indicate metallic properties for $BaIr_2Ge_2$, and electronic structure calculations are consistent with the observed behavior. Future efforts will be focused on inducing a metal-insulator transition in $BaIr_2Ge_2$.

Supplementary Materials: The following are available online at www.mdpi.com/1996-1944/10/7/818/s1, Table S1: SEM-EDX, Table S2: Anisotropic Thermal Parameters of $BaIr_2Ge_2$ from single crystal diffraction.

Acknowledgments: This research at LSU was supported by LSU-startup funding and the Louisiana Board of Regents Research Competitiveness Subprogram (RCS) under Contract Number LEQSF (2017-20)-RD-A-08. T.-R. Chang was supported by the Ministry of Science and Technology and National Cheng Kung University, Taiwan. T.-R. Chang also thanks National Center for Theoretical Sciences (NCTS), Taiwan for technical support. The physical property characterization at Princeton University was supported by the Department of Energy, Division of Basic Energy Sciences, grant DE-FG02-98ER45706.

Author Contributions: W.X. conceived and designed the experiments; X.G. and M.T.P. performed the experiments; R.J.C. and T.K. contributed physical properties measurements. T.-R.C. contributed electronic structure calculations; all the authors wrote the paper.

Conflicts of Interest: The authors declare no conflict of interest.

References

1. Margadonna, S.; Takabayashi, Y.; Mcdonald, M.T.; Kasperkiewicz, K.; Mizuguchi, Y.; Takano, Y.; Fitch, A.N.; Suard, E.; Prassides, K. Crystal structure of the new $FeSe_{1-x}$ superconductor. *Chem. Commun.* **2008**, *43*, 5607–5609. [CrossRef] [PubMed]
2. Lee, K.-W.; Pardo, V.; Pickett, W.E. Magnetism driven by anion vacancies in superconducting α-$FeSe_{1-x}$. *Phys. Rev. B* **2008**, *78*, 174502. [CrossRef]
3. Okada, H.; Igawa, K.; Takahashi, H.; Kamihara, Y.; Hirano, M.; Hosono, H.; Matsubayashi, K.; Uwatoko, Y. Superconductivity under high pressure in LaFeAsO. *J. Phys. Soc. Jpn.* **2008**, *77*, 113712. [CrossRef]
4. Rotter, M.; Tegel, M.; Johrendt, D. Superconductivity at 38 K in the iron arsenide $(Ba_{1-x}K_x)Fe_2As_2$. *Phys. Rev. Lett.* **2008**, *101*, 107006. [CrossRef] [PubMed]
5. Gor'kov, L.P.; Grüner, G. *Charge Density Waves in Solids*, 1st ed.; North Holland: Amsterdam, The Netherlands, 1989; pp. 1–494. ISBN 9780444600738.
6. Gruner, G. *Density Waves in Solids*; reprint; Westview Press: Boulder, CO, USA, 2009; pp. 1–288. ISBN 9780786747795.
7. Lin, Q.; Miller, G.J.; Corbett, J.D. Ordered $BaAl_4$-type variants in the $BaAu_xSn_{4-x}$ system: A unified view on their phase stabilities versus valence electron counts. *Inorg. Chem.* **2014**, *53*, 5875–5877. [CrossRef] [PubMed]
8. Häussermann, U.; Amerioun, S.; Eriksson, L.; Lee, C.-S.; Miller, G.J. The s–p bonded representatives of the prominent $BaAl_4$ structure type: A case study on structural stability of polar intermetallic network structures. *J. Am. Chem. Soc.* **2002**, *124*, 4371–4383. [CrossRef] [PubMed]
9. Hoffmann, R.; Zheng, C. Making and breaking bonds in the solid state: The thorium chromium silicide ($ThCr_2Si_2$) structure. *J. Phys. Chem.* **1985**, *89*, 4175–4181. [CrossRef]
10. Zheng, C.; Hoffmann, R. Donor-acceptor layer formation and lattice site preference in the solid: The $CaBe_2Ge_2$ structure. *J. Am. Chem. Soc.* **1986**, *108*, 3078–3088. [CrossRef]
11. Tan, X.; Fabbris, G.; Haskel, D.; Yaroslavtsev, A.A.; Cao, H.; Thompson, C.M.; Kovnir, K.; Menushenkov, A.P.; Chernikov, R.V.; Garlea, V.O.; et al. Transition from localized to strongly correlated electron behavior and mixed valence driven by physical or chemical pressure in ACo_2As_2 (A = Eu and Ca). *J. Am. Chem. Soc.* **2016**, *138*, 2724–2731. [CrossRef] [PubMed]
12. Kudo, K.; Nishikubo, Y.; Nohara, M. Coexistence of superconductivity and charge density wave in $SrPt_2As_2$. *J. Phys. Soc. Jpn.* **2010**, *79*, 123710. [CrossRef]
13. Settaia, R.; Sugitania, I.; Okudaa, Y.; Thamizhavela, A.; Nakashimab, M.; Onukia, Y.; Harimac, H. Pressure-induced superconductivity in $CeCoGe_3$ without inversion symmetry. *J. Magn. Magn. Mater.* **2007**, *310*, 844–846. [CrossRef]
14. Samokhin, K.V.; Zijlstra, E.S.; Bose, S.K. $CePt_3Si$: An unconventional superconductor without inversion center. *Phys. Rev. B* **2004**, *69*, 094514. [CrossRef]
15. Kovnir, K.A.; Zaikina, J.V.; Reshetova, L.N.; Olenev, A.V.; Dikarev, E.V.; Shevelkov, A.V. Unusually high chemical compressibility of normally rigid type-I clathrate framework: Synthesis and structural study of $Sn_{24}P_{19.3}Br_xI_{8-x}$ solid solution, the prospective thermoelectric material. *Inorg. Chem.* **2004**, *43*, 3230–3236. [CrossRef] [PubMed]
16. Kim, S.-J.; Hu, S.; Uher, C.; Hogan, T.; Huang, B.; Corbett, J.D.; Kanatzidis, M.G. Structure and thermoelectric properties of Ba_6Ge_{25-x}, $Ba_6Ge_{23}Sn_2$, and $Ba_6Ge_{22}In_3$: Zintl phases with a chiral clathrate structure. *J. Solid State Chem.* **2000**, *153*, 321–329. [CrossRef]
17. Fukuoka, H.; Kiyoto, J.; Yamanaka, S. Superconductivity and crystal structure of the solid solutions of $Ba_{8-d}Si_{46-x}Ge_x$ ($0 \leq x \leq 23$) with Type I clathrate structure. *J. Solid State Chem.* **2003**, *175*, 237–244. [CrossRef]
18. Klemm, W. Centenary-Lecture-Metalloids and their Compounds with the Alkali Metals. *Proc. Chem. Soc. Lond.* **1958**, *12*, 329–341.

19. Mott, N.F. *Metal-Insulator Transitions*, 2nd ed.; Taylor & Francis Inc.: London, UK, 1990; pp. 1–34. ISBN 0-85066-783-6.
20. Kakihana, M.; Akamine, H.; Tomori, K.; Nishimura, K.; Teruya, A.; Nakamura, A.; Honda, F.; Aoki, D.; Nakashima, M.; Amako, Y.; et al. Superconducting, Fermi surface, and magnetic properties in $SrTGe_3$ and $EuTGe_3$ (T: Transition metal) with the Rashba-type tetragonal structure. *J. Alloys Compd.* **2017**, *694*, 439–451. [CrossRef]
21. Petříček, V.; Dušek, M.; Palatinus, L. Crystallographic computing system JANA2006: General features. *Z. Kristallogr. Cryst. Mater.* **2014**, *229*, 345–352. [CrossRef]
22. Sheldrick, G.M. A short history of *SHELX*. *Acta Crystallogr. Sect. A: Found. Crystallogr.* **2008**, *64*, 112–122. [CrossRef] [PubMed]
23. Bruker. *Smart*; Bruker AXS Inc.: Madison, WI, USA, 2012. Available online: https://www.bruker.com/products/x-ray-diffraction-and-elemental-analysis/single-crystal-x-ray-diffraction/sc-xrd-software/overview/sc-xrd-software/apex3.html (accessed on 12 July 2017).
24. Hohenberg, P.; Kohn, W. Inhomogeneous electron gas. *Phys. Rev.* **1964**, *136*, B864. [CrossRef]
25. Perdew, J.P.; Burke, K.; Ernzerhof, M. Generalized gradient approximation made simple. *Phys. Rev. Lett.* **1996**, *77*, 3865–3868. [CrossRef] [PubMed]
26. Fujii, H.; Sato, A. Crystal structure of ternary germanides SrM_2Ge_2 (M = Ni and Ir). *J. Alloys Compd.* **2009**, *487*, 198–201. [CrossRef]
27. Siggelkow, L.; Hlukhyy, V.; Fässler, T.F. Synthesis, Structure and chemical bonding of $CaCo_2Si_2$ and $BaCo_2Ge_2$—Two new compounds with $ThCr_2Si_2$ Structure type. *Z. Anorg. Allg. Chem.* **2010**, *636*, 378–384. [CrossRef]
28. Venturini, G.; Malaman, B. X-ray single crystal refinements on some RT_2Ge_2 compounds (R = Ca, Y, La, Nd, U; T = Mn-Cu, Ru-Pd): Evolution of the chemical bonds. *J. Alloys Compd.* **1996**, *235*, 201–209. [CrossRef]
29. Venturini, G.; Malaman, B.; Roques, B. Contribution a la cristallochimie des isotypes de $ThCr_2Si_2$ et $CaBe_2Ge_2$: II. Variation des distances interatomiques dans des germaniures MM'_2Ge_2 de type $ThCr_2Si_2$ (M = Y, Nd, Ca; M' = Mn, Cu, Ru, Rh, Pd, Ir). *J. Solid State Chem.* **1989**, *79*, 136–145. [CrossRef]
30. González, J.; Kessens, R.; Schuster, H.U. Darstellung und kristallstruktur neuer AM_2X_2-verbindungen in den systemen erdalkalimetall-platinmetall-germanium. *Z. Anorg. Allg. Chem.* **1993**, *619*, 13–16. [CrossRef]
31. Hlukhyy, V.; Hoffmann, A.V.; Fässler, T.F. Synthesis, structure and chemical bonding of $CaFe_{2-x}Rh_xSi_2$ (x = 0, 1.32, and 2) and $SrCo_2Si_2$. *J. Solid State Chem.* **2013**, *203*, 232–239. [CrossRef]
32. Doerrscheidt, W.; Niess, N.; Schaefer, H. Neue verbindungen AB_2X_2 (A = Erdalkalimetall, B = Uebergangselement, X = Element (IV)) im $ThCr_2Si_2$-Typ. *Z. Naturforsch. B* **1976**, *31*, 890–891.
33. May, N.; Mueller, W.; Schaefer, H. Ternäre erdalkali-beryllium-silicide und -germanide mit AlB_2-struktur. ternary alkaline-earth-beryllium-silicides and -germanides of AlB_2-structure. *Z. Naturforsch. B* **1974**, *29*, 325–327. [CrossRef]
34. Langen, D.; Schoolaert, S.; Ploss, H.; Jung, W. Die isotypen verbindungen $BaRh_2Si_2$, $BaIr_2Si_2$ und $BaPt_2Ga_2$-eine monokline verzerrungsvariante der $CaRh_2B_2$-strukur. *Z. Anorg. Allg. Chem.* **1997**, *623*, 1561–1566. [CrossRef]
35. Falmbigl, M.; Grytsiv, A.; Rogl, P.; Giester, G. Clathrate formation in the systems Ba-Ir-Ge and Ba-{Rh, Ir}-Si: Crystal chemistry and phase relations. *Intermetallics* **2013**, *36*, 61–72. [CrossRef]
36. Nasir, N.; Melnychenko-Koblyuk, N.; Grytsiv, A.; Rogl, P.; Giester, G.; Wosik, J.; Nauer, G.E. Ternary systems Sr-{Ni, Cu}-Si: Phase equilibria and crystal structure of ternary phases. *J. Solid State Chem.* **2010**, *183*, 565–574. [CrossRef]
37. Baelus, B.J.; Peeters, F.M.; Schweigert, V.A. Saddle-point states and energy barriers for vortex entrance and exit in superconducting disks and rings. *Phys. Rev. B* **2001**, *63*, 144517. [CrossRef]